文章编号：1001-9014(2022)01-0294-05

DOI:10.11972/j.issn.1001-9014.2022.01.024

A millimeter-wave fast imaging algorithm with range compensation for one-stationary bistatic SAR

CHEN Xu, YANG Qi, ZENG Yang*, WANG Hong-Qiang, DENG Bin

(College of Electronic Science and Technology, National University of Defense Technology, Changsha 410073, China)

Abstract: In this article, an improved millimeter-wave fast imaging algorithm with range compensation for one-stationary bistatic synthetic aperture radar (OS-BiSAR) is presented. During the process of image reconstruction, the amplitude attenuation factor of the echo model is retained for the compensation of signal propagation loss, and the convolution operation is performed on the receiving array dimension according to the characteristics of the target echo equation. Finally, the target image can be solved by fast Fourier transform (FFT) and coherent accumulation steps. Simulation analysis and experimental results show that, compared to the range migration algorithm (RMA) with range compensation, the proposed algorithm can not only guarantee the efficiency of image reconstruction, but also significantly reduce the influence of signal propagation loss on the image quality.

Key words: millimeter-wave fast imaging algorithm, range compensation, one-stationary bistatic synthetic aperture radar (OS-BiSAR), fast Fourier transform (FFT)

一端固定的双站SAR体制下基于距离补偿的毫米波快速成像算法

陈 旭，杨 琪，曾 旸*，王宏强，邓 彬

（国防科技大学电子科学学院，湖南 长沙 410073）

摘要：本文提出了一种一端固定的双站SAR(OS-BiSAR)体制下基于距离补偿的毫米波快速成像算法。在图像重构过程中，该算法通过保留回波模型中的幅度衰减因子来补偿信号传播衰减，并根据目标回波方程特性对接收阵列维执行了卷积操作，最后通过快速傅里叶变换(FFT)以及相干累加等步骤求解出最终目标图像。仿真分析和实验结果表明，与OS-BiSAR体制下基于距离补偿的距离徙动算法(RMA)相比，所提算法不仅可以保证图像重构效率，还能更显著地降低信号沿空间路径的传播损耗对成像质量带来的影响。

关 键 词：毫米波快速成像算法；距离补偿；一端固定的双站SAR；快速傅里叶变换

中图分类号：TN95　　**文献标识码**：A

Introduction

Different from X-ray, millimeter-wave can not only penetrate clothing and other media materials, but also ensure human life, health and safety. Moreover, millimeter-wave can also achieve high-resolution imaging. Therefore, active millimeter-wave imaging technology can be widely used in civil fields such as security check and medical imaging[1-2]. Most of the existing active millimeter-wave imaging systems are based on monostatic synthetic aperture radar[3]. However, the reconstructed image quality depends on the target shape for a given array length[4]. In contrast, the application of one-stationary bistatic synthetic aperture radar (OS-BiSAR) can not only collect more target information, but also weaken the coupling effect of transceiver antenna[5-6].

OS-BiSAR, also known as bistatic parasitic SAR[7], is a BiSAR in which only one of the transmitters and receivers mechanically scans to form an azimuth synthetic aperture, while the other is in a static state. A high-precision OS-BiSAR range migration algorithm (RMA) was proposed in Ref. [8], and the analytical two-dimensional (2-D) spectrum was derived without any approximation. However, in the near-field environment, the detect-

Received date: 2021-03-10, **revised date**: 2021-11-01　　**收稿日期**：2021-03-10，**修回日期**：2021-11-01

Foundation items: Supported by the National Natural Science Foundation of China (61871386, 62035014, 61921001).

Biography: Chen Xu (1995-), male, Baicheng, doctor. Research area involves millimeter-wave imaging, radar adaptive waveform design and signal processing. E-mail: xuchen95909@126.com.

* **Corresponding author**: E-mail: zengyang@nudt.edu.cn

able range of the imaging system is usually in the same order as the distance between the target and the array plane, so the imaging quality of the distant target is inevitably affected by the signal propagation loss. Back-projection algorithm is a typical imaging algorithm that can be applied to OS-BiSAR system[9]. Although it can eliminate the influence of signal propagation loss on the reconstructed image quality through matched filtering, the huge amount of computation brought by the application of this method leads to extremely low imaging efficiency. According to the principles of equivalent phase center and scalar diffraction theory, Wang et al. proposed a multiple-input multiple-output RMA with range compensation, but the quality of reconstructed image will be reduced by this method[10]. Then, a more effective RMA with range compensation for OS-BiSAR is proposed in Ref. [11]. In this algorithm, the amplitude factor is considered in the process of Fourier transform, which can effectively compensate the propagation loss on the premise of ensuring high imaging efficiency. However, the plane-wave approximation introduced in this algorithm leads to the partial loss of the attenuation compensation factor, so the loss compensation ability of this method for distant targets is still limited.

In this article, an improved fast imaging algorithm with range compensation for OS-BiSAR is proposed. During the implementation of this algorithm, the target image is decomposed into multiple sub-images and the FFT-based imaging scheme is adopted, which means that the proposed algorithm can not only ensure the efficiency and quality of the target image reconstruction, but also significantly improve the performance of range compensation.

1　Signal model for the near-field OS-BiSAR

The imaging geometry of the near-field OS-BiSAR is shown in Fig. 1, in which the transmitter and receiver are separated. In this system, the transmitter element is fixed, and the receiver is mechanically scanned in the azimuth direction to form a synthetic aperture. In order to simplify the analysis, it is assumed that the transmitter and the receivers are located on the plane of $z = z_0$, and the corresponding coordinates are $\left(0, y_{T0}, z_0\right)$ and $\left(x_R, 0, z_0\right)$ respectively. The spacial target (x, y, z) is located on the plane of $y = 0$, and the corresponding electromagnetic reflectivity is $\sigma(x, z)$. R_t is the distance between the target and the transmitter, and R_r is the distance between the target and the receiver, which can be respectively expressed as:

$$R_t = \sqrt{x^2 + {y_{T0}}^2 + \left(z - z_0\right)^2} \quad , \quad (1)$$

$$R_r = \sqrt{\left(x - x_R\right)^2 + \left(z - z_0\right)^2} \quad . \quad (2)$$

Through considering the signal propagation loss, the amplitude attenuation factor $1/\left(R_t R_r\right)$ is introduced into the echo model. Assuming that the transmitter transmits wide-band signal, the echo model can be expressed as:

$$s\left(k, x_R\right) = \iint \sigma\left(x, z\right) \cdot \frac{1}{R_t R_r} \cdot e^{-jk\left(R_t + R_r\right)} dx dz \quad . \quad (3)$$

In the above formula, $k = 2\pi f/c$ is the spatial wave number, in which f and c denote the frequency and the light speed respectively.

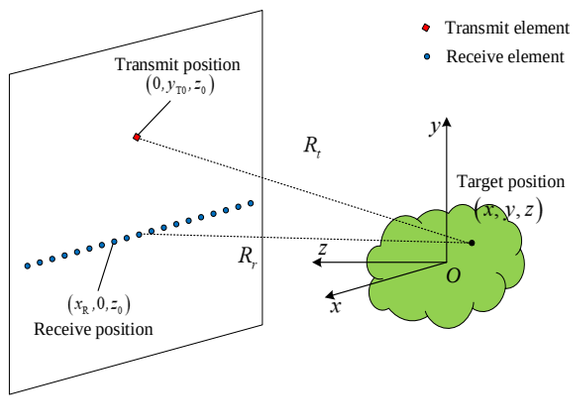

Fig. 1　Imaging geometry of the near-field OS-BiSAR
图1　近场OS-BiSAR成像几何

2　Improved fast imaging algorithm with range compensation

Define

$$\bar{\sigma}\left(k, x, z\right) = \sigma\left(x, z\right) \cdot \frac{1}{R_t} \cdot \mathrm{e}^{-jkR_t} \quad , \quad (4)$$

$$F(k, x - x_R, z) = \frac{1}{R_r} \cdot \mathrm{e}^{-jkR_r} \quad . \quad (5)$$

Then, (3) can be rewritten as

$$s\left(k, x_R\right) = \iint \bar{\sigma}\left(k, x, z\right) \cdot F(k, x - x_R, z) \mathrm{d}x \mathrm{d}z \quad . \quad (6)$$

According to the principle of matched filtering[12], the approximate target image can be represented as:

$$\bar{\sigma}\left(k, x, z\right) = \int s\left(k, x_R\right) \cdot F^{-1}(k, x - x_R, z) \mathrm{d}x_R \quad . \quad (7)$$

The relation between $F^{-1}(k, x - x_R, z)$ and $F(k, x - x_R, z)$ is

$$F^{-1}(k, x - x_R, z) * F(k, x - x_R, z) = \delta(k, x - x_R, z) \quad . \quad (8)$$

In the above formula, $*$ and $\delta(\cdot)$ represent the convolution symbol and the impulse function respectively. It can be seen that (7) is the convolution integral expression of x_R, which can be transformed into

$$\bar{\sigma}\left(k, x, z\right) = s\left(k, x\right) *_{(x)} F^{-1}(k, x, z) \quad . \quad (9)$$

Time domain convolution is equivalent to frequency domain multiplication. Then, the fast Fourier transform (FFT) operation is performed on x dimension of (9)

$$\bar{\sigma}\left(k, k_x, z\right) = s\left(k, k_x\right) \cdot F^{-1}(k, k_x, z) \quad . \quad (10)$$

For each spatial wave-number k_l, we can get

$$\bar{\sigma}_{k_l}\left(k_x, z\right) = s\left(k_l, k_x\right) \cdot F^{-1}(k_l, k_x, z) \quad . \quad (11)$$

The sub-image corresponding to k_l can be obtained by performing inverse FFT operation on k_x dimension of Eq. (11)

$$\bar{\sigma}_{k_l}(x,z) = \mathrm{IFFT}_{(k_x)}\left[s\left(k_l,k_x\right) \cdot F^{-1}(k_l,k_x,z)\right]. \quad (12)$$

Then, the amplitude and phase compensation are performed on each sub-image $\bar{\sigma}_{k_l}(x,z)$ according to Eq. (4)

$$\hat{\sigma}_{k_l}(x,z) = \bar{\sigma}_{k_l}(x,z) \cdot R_t \cdot \mathrm{e}^{\mathrm{j}k_l R_t} \quad . \quad (13)$$

The final target image can be obtained by coherent accumulation of all the sub-images

$$\hat{\sigma}(x,z) = \sum_{l=1}^{N} \hat{\sigma}_{k_l}(x,z) \quad . \quad (14)$$

In the above formula, N denotes the number of spatial wave-number. Therefore, the steps of improved fast imaging algorithm with range compensation for OS-BiSAR are as follows:

(1) Performing FFT operation on $x_{\mathrm{R}}$of the 2-D spatial echo signal $s\left(k,x_{\mathrm{R}}\right)$ respectively, and the spectral echo signal $\bar{s}\left(k,k_x\right)$ can be obtained.

(2) Establishing the expression $G(k,x_{\mathrm{R}},z)$ which contains the amplitude and phase terms

$$G(k,x_{\mathrm{R}},z) = \sqrt{{x_{\mathrm{R}}}^2 + \left(z-z_0\right)^2} \cdot \mathrm{e}^{\mathrm{j}k\sqrt{{x_{\mathrm{R}}}^2+\left(z-z_0\right)^2}}. \quad (15)$$

(3) Performing FFT operation on the height dimension x_{R} of $G(k,x_{\mathrm{R}},z)$ to obtain $\bar{G}(k,k_x,z)$.

(4) For each spatial wave-number k_l, define $M\left(k_l,k_x,z\right) = \bar{s}\left(k_l,k_x\right) \cdot \bar{G}(k_l,k_x,z)$.

(5) IFFT operation is performed on $k_x$of $M\left(k_l,k_x,z\right)$ to obtain the sub-image $\bar{\sigma}_{k_l}(x,z)$ corresponding to the spatial wave-number k_l.

(6) Performing the amplitude and phase compensation for each sub-image $\bar{\sigma}_{k_l}(x,z)$, and the corrected sub-image can be obtained by $\hat{\sigma}_{k_l}(x,z) = \bar{\sigma}_{k_l}(x,z) \cdot \sqrt{x^2+{y_{\mathrm{T0}}}^2+\left(z-z_0\right)^2} \cdot e^{\mathrm{j}k_l\sqrt{x^2+{y_{\mathrm{T0}}}^2+\left(z-z_0\right)^2}}$.

(7) The final target image $\hat{\sigma}(x,z)$ can be reconstructed by the coherent summation of all the target sub-images $\hat{\sigma}_{k_l}(x,z)$.

Assuming that the magnitude of each variable is N, and the computational complexity of the proposed algorithm can be estimated to be $O\left(N^3\log_2 N\right)$ according to the above process. In contrast, the computational complexity of OS-BiSAR RMA with range compensation in Ref. [11] is $O\left(N^2\log_2 N\right)$. However, the computational complexity of these two algorithms will not represent the actual amount of computation and running time. Next, the effectiveness of the proposed algorithm will be verified by simulation analysis and experimental results.

3 Simulation analysis

In this article, the OS-BiSAR RMA with range compensation is used to compare with the proposed algorithm, and then the effectiveness of the proposed algorithm in compensating signal propagation attenuation can be verified. All the imaging algorithms were implemented on a computer with 2.1 GHz processor and 8 GB memory. In the OS-BiSAR imaging system, the length of the receiving array is 0.486 m, where the spacing of the array elements is set to 6mm. The frequency range of the transmitted signal is set to 26.5 GHz to 40 GHz, and the number of sampling points is 101.

As shown in Fig. 2(a), the imaging targets are 15 ideal scattering points uniformly distributed on the plane of $y = 0$. The corresponding imaging results of these two algorithms are presented in Fig. 2(b) and Fig. 2(c) respectively. The imaging dynamic range is set to 10 dB, and the imaging time of these two algorithms is 0.24 s and 0.61 s respectively. Since the near-field echo data recorded by the OS-BiSAR system is in 2-D, the amount of data is not large, the absolute time difference between these two algorithms is not significant, and both can meet the requirements of real-time imaging. In addition, by applying parallel computation with GPU, the sub-image corresponding to each spatial wave-number can be reconstructed at the same time. This can further reduce the imaging time of our proposed method by a factor of 1/N.

It can be seen from Fig. 2(b) that the pixel intensity of the targets at $z = 0.9$ m is significantly weaker than that of the targets at $z = 0.5$ m. However, in Fig. 2(c), the pixel intensity of the point targets on different z planes is almost the same, which indicates that the proposed algorithm has better loss compensation performance. It is worth mentioning that the compensation value of the proposed algorithm for spacial electromagnetic signal attenuation is $\sqrt{{x_{\mathrm{R}}}^2+\left(z-z_0\right)^2} \cdot \sqrt{x^2+{y_{\mathrm{T0}}}^2+\left(z-z_0\right)^2}$, while the OS-BiSAR RMA with range compensation is $\sqrt{\left(z-z_0\right)} \cdot \sqrt{x^2+{y_{\mathrm{T0}}}^2+\left(z-z_0\right)^2}$. The lost in the amplitude results in the reduced pixel value of remote targets or targets of low RCSs.

4 Experimental results

In this article, an OS-BiSAR experimental system is built to verify the feasibility of the proposed method in practical application. In this system, the length of the receiving array is 0.3 m, where the spacing of the array elements is set to 9 mm. The frequency range of the transmitted signal is set to 30 GHz to 36 GHz, and the number of sampling points is 101.

The imaging scene is shown in Fig. 3(a), in which the imaging targets are a corner reflector and a metal ball at different distances. The corresponding imaging results of OS-BiSAR RMA with range compensation and the proposed algorithm are presented in Fig. 3(b) and Fig. 3(c) respectively. The imaging dynamic range is also set to 10 dB, and the imaging time of these two algorithms is 0.12 s and 0.39 s respectively. It can be seen from Fig. 3(b) that the pixel value intensity of the far ball is weaker than that of the near corner reflector, and the range compensation performance of the proposed algorithm is much better.

In order to quantitatively analyze the attenuation compensation effect of the proposed method for different targets, the azimuth profiles of the experimental scene

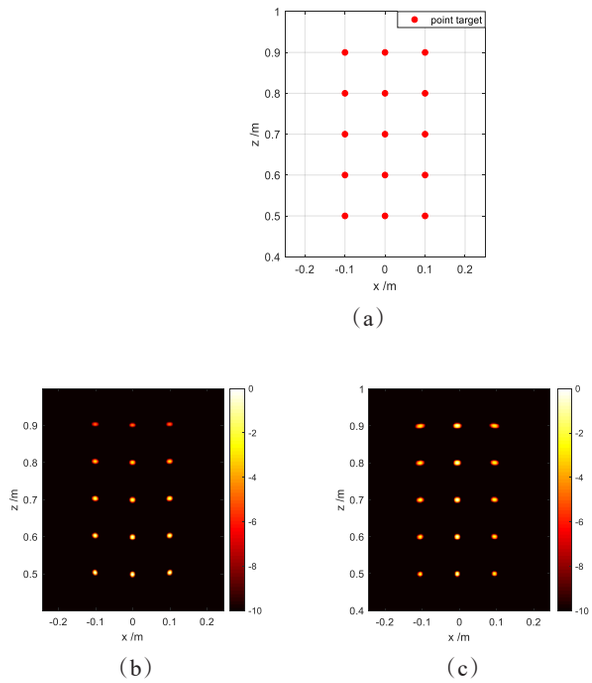

Fig. 2　Imaging results of the target model of multiple points, (a) the target model of multiple scattering points, (b) imaging result of OS-BiSAR RMA with range compensation, (c) imaging result of the proposed algorithm.
图2　多点目标模型成像结果 (a) 理想散射点目标模型,(b) OS-BiSAR体制下基于距离补偿的RMA重构结果,(c) 所提算法重构结果

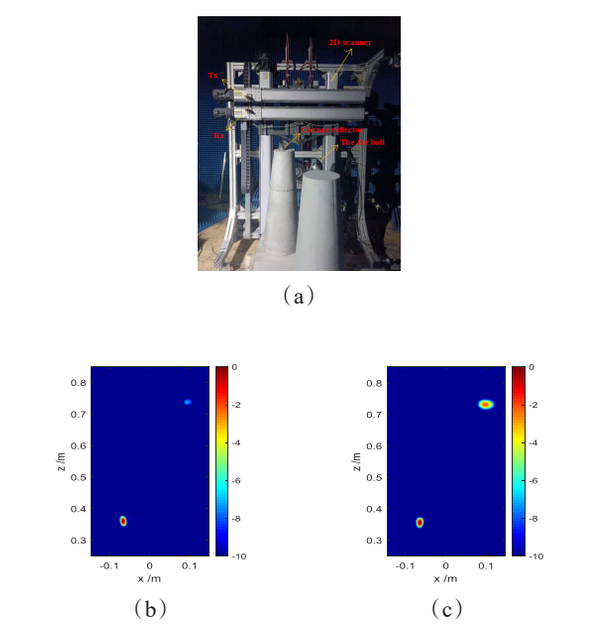

Fig. 3　Experimental results of the corner reflector and the metal ball at different distances, (a) imaging scene, (b) imaging result of OS-BiSAR RMA with range compensation, (c) imaging result of the proposed algorithm.
图3　目标为位于不同距离的角反射器和金属小球的实验成像结果,(a) 成像场景,(b) OS-BiSAR体制下基于距离补偿的RMA重构结果,(c) 所提算法重构结果

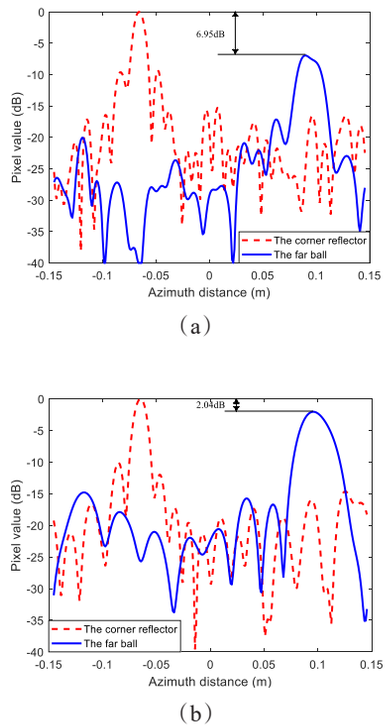

Fig. 4　Azimuth profiles of the corner reflector and the far ball by using (a) OS-BiSAR RMA with range compensation and (b) the proposed algorithm
图4　通过使用(a)OS-BiSAR体制下基于距离补偿的RMA和(b)所提算法得到的角反射器和远处金属小球的方位像结果

obtained by using OS-BiSAR RMA with range compensation and the proposed algorithm are presented in Fig. 4 (a) and Fig. 4(b) respectively. It can be seen that the pixel intensity attenuation of the far ball by using OS-BiSAR RMA with range compensation is 6. 95 dB, while the proposed algorithm is only 2. 04 dB.

5　Conclusion

In this article, an improved millimeter-wave fast imaging algorithm with range compensation for OS-BiSAR has been proposed. From the above analysis, it can be seen that compared with OS-BiSAR RMA with range compensation, the proposed algorithm not only avoids multi-step approximation and interpolation operations, but also significantly reduces the influence of signal propagation loss on the imaging quality while ensuring the reconstruction efficiency. It will provide useful guidance for the imaging of long-distance weak targets under near-field conditions. Further developments of fast imaging algorithms with range compensation for MIMO-SAR and cross-MIMO array are planned for the imaging of complex targets such as mannequin and models of vehicles.

Acknowledgment

Project supported by the National Natural Science Foundation of China (Grant No. 61871386, No.

62035014 and No. 61921001)

References

[1] Zhuge X, Yarovoy A G. A sparse aperture MIMO-SAR-Based UWB imaging system for concealed weapon detection[J]. *IEEE Transactions on Geoscience and Remote Sensing*, 2010, **49**(1):509-518.

[2] Alvarez Y, Gonzalez-Valdes B, José ngel Martinez, *et al*. 3D whole body imaging for detecting explosive-related threats[J]. *IEEE Transactions on Antennas and Propagation*, 2012, **60**(9):4453-4458.

[3] Sheen D M, Mcmakin D L, Hall T E. Three-dimensional millimeter-wave imaging for concealed weapon detection[J]. *IEEE Transactions on Microwave Theory Techniques*, 2001, **49**(9):1581-1592.

[4] Ashkan F A, Zahra K, Mahdi S. Efficient millimetre-wave imaging structure for detecting axially rotated objects[J]. *IET Microwaves Antennas & Propagation*, 2018, **12**(3):416-424.

[5] Manzoor Z, Ghasr M T, Donnell K M. Image distortion characterization due to equivalent monostatic approximation in near-field bistatic SAR imaging[J]. *IEEE Transactions on Instrumentation and Measurement*, 2020, **69**(7):4898-4907.

[6] Wu J, Li Z, Huang Y, *et al*. Omega-K imaging algorithm for one-stationary bistatic SAR[J]. *IEEE Transactions on Aerospace and Electronic Systems*, 2014, **50**(1):33-52.

[7] Cazzani L, Colesanti C, Leva D, *et al*. A ground-based parasitic SAR experiment[J]. *IEEE Transactions on Geoscience and Remote Sensing*, 2002, **38**(5):2132-2141.

[8] Zeng T, Liu F, Hu C, *et al*. Image formation algorithm for asymmetric bistatic SAR systems with a fixed receiver[J]. *IEEE Transactions on Geoscience and Remote Sensing*, 2012, **50**(11):4684-4698.

[9] Demirci S, Cetinkaya H, Yigit E, *et al*. A study on millimeter-wave imaging of concealed objects: Application using back-projection algorithm[J]. *Progress in Electromagnetics Research*, 2012, **128**(1):457-477.

[10] Wang Z, Guo Q, X Tian, *et al*. Near-field 3-D millimeter-wave imaging using MIMO RMA with range compensation[J]. *IEEE Transactions on Microwave Theory and Techniques*, 2019, **67**(3):1157-1166.

[11] Wang Z, Guo Q, Tian X, *et al*. Millimeter-Wave image reconstruction algorithm for one-stationary bistatic SAR[J]. *IEEE Transactions on Microwave Theory and Techniques*, 2020, **68**(3):1185-1194.

[12] Laviada J, Arboleya-Arboleya A, Las-Heras F. Multistatic millimeter-wave imaging by multiview portable camera[J]. *IEEE Access*, 2017, **5**:19259-19268.